Geoscience Frontiers 12 (2021) 983–989

HOSTED BY

Contents lists available at ScienceDirect

Geoscience Frontiers

journal homepage: www.elsevier.com/locate/gsf

Research Paper

The effect of nitrogen on the compressibility and conductivity of iron at high pressure

HPSTAR 1134-2021

Yukai Zhuang [a], Xiaowan Su [b], Nilesh P. Salke [a], Zhongxun Cui [a], Qingyang Hu [a], Dongzhou Zhang [c], Jin Liu [a,*]

[a] Center for High Pressure Science and Technology Advanced Research (HPSTAR), Beijing 100094, China
[b] School of Earth and Space Sciences, Peking University, Beijing 100871, China
[c] Hawai'i Institute of Geophysics and Planetology, School of Ocean and Earth Science and Technology, University of Hawai'i at Manoa, Honolulu, HI, 96822, USA

ARTICLE INFO

Keywords:
High pressure
Iron nitrides
Synchrotron X-ray diffraction
Electrical conductivity

ABSTRACT

Although nitrogen in the Earth's interior has attracted significant attention recently, it remains the most enigmatic of the light elements in the Earth's core. In this work, synchrotron X-ray diffraction (XRD) and electrical conductivity experiments were conducted on iron nitrides (Fe_2N and Fe_4N) in diamond anvil cells (DACs) up to about 70 GPa at ambient temperature. These results show that iron nitrides are stable up to at least 70 GPa. From the equation of state (EOS) parameters, iron nitrides are more compressible than iron carbides. Moreover, using the van der Pauw method and Wiedemann-Franz law, the electrical and thermal conductivity of samples were determined to be much lower than that of iron carbides. The conductivities of Fe_2N and Fe_4N were similar at 20–70 GPa, suggesting no evident effects by varying the N stoichiometries in iron nitrides. Iron nitrides are less dense and conductive but more compressible than carbides at 0–70 GPa. This study indicates that less nitrogen than carbon can explain geophysical phenomena in the deep Earth, such as the density deficit.

1. Introduction

Nitrogen, the fifth most abundant element in the Solar System, is highly significant in life as well as to our planet (Bebout et al., 2013). Compared to other terrestrial planets like Venus and Mars, the anomalously high nitrogen content in Earth's atmosphere might be linked to the distinctive nitrogen progresses on Earth, such as life evolution and plate tectonics (Owen et al., 1977; Lécuyer et al., 2000). While N_2 is the primary constituent in our planet's atmosphere, iron nitrides are likely stored throughout all geological reservoirs in the Earth's interior. However, the storage and circulation of deep nitrogen remain hotly debated (Halliday, 2013). To date, nitrogen is one of the least studied elements under conditions relevant to the Earth's deep interior (Litasov et al., 2014).

Based on its high volatility and low concentration in some meteorites, it is largely presumed that nitrogen is only abundant on the Earth's surface but scantly in the deep Earth (Allègre et al., 2001). It is evident that negligible nitrogen concentrations (several ppm) are in some stony meteorites (Sugiura et al., 1998). On the other hand, the primary building blocks of Earth (i.e., enstatite and carbonaceous chondrites) and many other meteorites can contain much more nitrogen ranging from a few hundred ppm to even more than 1000 ppm (Moore and Keil, 1969; Javoy, 1997). For instance, Sugiura et al. (1998) found that the amount of nitrogen in the taenite portion of iron meteorites can be up to 1 wt.%. The nitrogen content of mantle-derived diamonds from kimberlites and metamorphic rocks could be up to 1500 ppm and 1.1 wt.%, respectively (Cartigny, 2005). Notably, Fe_4N (roaldite) has been observed in some iron meteorites (Rubin, 1997). Thus, iron meteorites can hold a substantial amount of nitrogen up to at least 1 wt.%, especially under reducing conditions (Adler and Williams, 2005).

The nitrogen content in the deep Earth may be significantly underestimated. Based on a chondritic comparison and terrestrial compilation, "missing N" reservoirs exist in the deep Earth (Johnson and Goldblatt, 2015). Johnson and Goldblatt (2015) proposed that the total mass of nitrogen in the Earth's mantle is likely about 2–6 times that of the atmosphere's N_2 (4×10^{18} kg) through subduction, while the core holds $\sim 10^{20}$ kg N. In particular, iron meteorites represent core remnants from differentiated and subsequently disintegrated planetesimals and they are

* Corresponding author.
E-mail address: jin.liu@hpstar.ac.cn (J. Liu).
Peer-review under responsibility of China University of Geosciences (Beijing).

https://doi.org/10.1016/j.gsf.2020.04.012
Received 13 November 2019; Received in revised form 22 January 2020; Accepted 22 April 2020
Available online 5 May 2020

mostly analogous to the central part of our planet. Thus, a small amount of the Earth's total N may remain on the Earth's surface, and the predominant portion could be hidden deep inside the Earth (Bebout and Penniston-Dorland, 2016; Yoshioka et al., 2018). Deep nitrogen is often considered to be N_2, NH_3, and its protonated form NH_4^+, which can substitute K^+, Na^+, and Ca^{2+} in silicate minerals (Eugster and Munoz, 1966; Watenphul et al., 2010; Mikhail and Sverjensky, 2014; Sokol et al., 2017b). In subduction zones, those forms of nitrogen would be mostly recycled back to the surface by slab-derived fluids, while a small portion could be delivered further into the deep mantle (Chen et al., 2019). However, these previous studies barely took into account the reaction of nitrogen with iron or the existence of iron nitrides in diamond inclusions. Due to their siderophile nature at high-pressure and high-temperature environments, iron nitrides are plausibly one of nitrogen's most common forms in the deep Earth (Johnson and Goldblatt, 2015; Bebout and Penniston-Dorland, 2016).

Thus far, Fe_7N_3 and Fe_3N have been extensively investigated. Hexagonal close-packed Fe_7N_3 could be stable up to at least 3000 K at 135 GPa (Adler and Williams, 2005; Kusakabe et al., 2019). Moreover, *ab initio* calculations predicted that Fe_7N_3 is dynamically and thermodynamically stable under the Earth's core conditions (Sagatov et al., 2019). In particular, β-Fe_7N_3 is structurally identical or very close to Fe_7C_3, including their elastic property (Minobe et al., 2015; Li et al., 2016). It is also suggested that carbon and nitrogen can mutually coexist and replace each other in the Earth's and other planetary cores (Sagatov et al., 2019). Meanwhile, another important type of iron nitride, Fe_3N, is stable to at least 30 GPa and 1473 K (Litasov et al., 2017). This phase could contain up to 2.5 wt.% C in equilibrium with C-rich melt, and the C-rich ε-Fe_3N nitride may be stable in local N-rich mantle domains, formed by redox freezing of N-rich carbonatite melts in the reduced mantle (Sokol et al., 2017a). Other iron nitrides such as Fe_2N and Fe_4N were primarily studied for their phase equilibria at only ambient pressure (Jacobs et al., 1995; Tessier et al., 2000). However, little is known about the high-pressure behavior of meteorite nitrogen components Fe_2N and Fe_4N (Nielsen and Buchwald, 1981; Sugiura, 1998). Therefore, it is indispensable to study the compressibility and conductivity properties of Fe_2N and Fe_4N at high pressure, allowing us a better understanding of the nature and role of these potential deep-nitrogen hosts in the Earth's deep interior (Adler and Williams, 2005; Kaminsky and Wirth, 2017).

In this study, the high-pressure stability and *P–V* EOS of Fe_2N and Fe_4N were determined using DACs coupled with synchrotron XRD. Further, conductivity measurements were carried on Fe_2N and Fe_4N samples up to 70 GPa at room temperature using the van der Pauw four-probe method. We found that both Fe_2N and Fe_4N significantly affect the geophysical properties of iron. Our results on Fe_2N and Fe_4N offer new insights into the evolution of iron nitrides with pressure and have been further applied to decipher the role of iron nitrides in the storage and circulation of deep nitrogen.

2. Materials and methods

Iron nitride powder samples were purchased from Beijing Antechnology Co., Ltd (Fe_2N Lot#: RA191101 and Fe_4N Lot#: RA191301) with lattice parameters of $a = 4.4181$ Å, $b = 5.4207$ Å, and $c = 4.7809$ Å for orthorhombic Fe_2N, and $a = 3.8023$ Å for cubic Fe_4N, respectively, based on in-house XRD measurements (Fig. S1). Polycrystalline samples were gently grounded and subsequently pressed between two opposing diamond anvils to form a disk of ~10 μm thick. The sample disk was then loaded into a DAC for further high-pressure measurements.

Synchrotron angular dispersive XRD experiments were carried out in a DAC with 200 μm culets at beamline 13BM-C of the GeoSoilEnviroCARS (GSECARS) at the Advanced Phonon Source (APS), Argonne National Laboratory (ANL). A monochromatic X-ray beam with a wavelength of 0.4340 Å was used to carry out the measurement. The incident X-ray beam was focused to a spot size of 15 μm × 15 μm, measured at the full width at half maximum. LaB_6 powder was used to calibrate the sample-to-detector distance, the tilt angle, and the rotation angle of the image plate relative to the incident X-ray beam. A MAR165 CCD detector was used to record diffracted X-rays. XRD images were collected at an exposure time of 120 s at intervals of ~1–3 GPa. A tungsten gasket was pre-indented to 40 μm thick with a hole of 100 μm in diameter drilled at the center to serve as the sample chamber. Neon was loaded into the sample chamber as the pressure-transmitting medium to provide quasi-hydrostatic conditions using the high-pressure gas loading system at the Center for High Pressure Science and Technology Advanced Research (HPSTAR). The pressure was calibrated using a ruby ball and a piece of Au placed next to the sample. The ruby pressure scale was crosschecked with the equation of state of Au (Mao et al., 1986; Ye et al., 2018). The pressure uncertainty was about 1–2 GPa throughout experiments. Diffraction patterns were integrated using the Dioptas program (Prescher and Prakapenka, 2015). The lattice parameters of the samples were derived using the UnitCell program. The EOS parameters obtained by fitting the *P–V* data to a third-order Birch-Murnaghan EOS:

$$P = \frac{3}{2}K_{T0}\left[\left(\frac{V_0}{V}\right)^{\frac{7}{3}} - \left(\frac{V_0}{V}\right)^{\frac{5}{3}}\right] \times \left\{1 + \frac{3}{4}\left(K_0^{'} - 4\right)\left[\left(\frac{V_0}{V}\right)^{\frac{2}{3}} - 1\right]\right\} \quad (1)$$

where P is pressure, K_{T0} is the isothermal bulk modulus at ambient pressure, V_0 and V are the volume at ambient conditions and high pressures, respectively, and $K_0^{'}$ is the pressure derivative of K_{T0} at 1 bar.

High-pressure four-probe electrical resistance experiments were carried out in a symmetrical DAC with 260 μm culet, coupled with a source meter (Keithley 2400) and a nanovoltage meter (Keithley 2182A) with an output current of ~1–5 mA at the HPSTAR. A tungsten gasket was pre-indented to 50 μm thick. A hole of 200 μm in diameter was drilled at the center of the indentation using laser ablation. Subsequently, the mixture of powder cubic boron nitride (cBN) and epoxy was packed into the hole and compressed to ~20 GPa, serving as a gasket insert. Afterwards, a hole of 70 μm in diameter was drilled at the center of the cBN gasket insert to act as an insulating sample chamber. Four Pt foils were used to serve as electrodes with 4 μm thick or less. The four-probe method can determine the resistivity of an arbitrary-shaped sample with an even thickness. It can also minimize the resistivity effect from the contact resistance, and the detailed process to obtain resistance was reported by van der Pauw (1958).

3. Results and discussion

3.1. Equation of state of Fe_2N and Fe_4N

XRD patterns of Fe_2N and Fe_4N were collected up to 65.4 and 71.4 GPa, respectively, at 300 K with 1–3 GPa intervals (Fig. 1). At ambient conditions, Fe_2N has an orthorhombic structure with space group *Pbcn* (Laniel et al., 2018), which persisted up to the highest pressure in our studies, as can be seen in Fig. 1a. Fe_4N crystallizes in a cubic structure with space group $Pm\bar{3}m$, consistent with previous work (Ishimatsu et al., 2003). Under pressure, Fe_4N remained stable in the pressure range of this experiment up to 71.4 GPa while we noted that the Fe_4N sample for high-pressure XRD measurements contained Fe_3N and Fe impurities (Fig. 1b), probably formed during the synthesis process of Fe_4N (Fig. S1). Adler and Williams (2005) had reported that the (200) diffraction peak of Fe_4N disappeared at ~30 GPa, which they claimed as a structural phase transition. However, we did not observe such a transition for Fe_4N in our experiments. Particularly, all diffraction peaks of Fe_4N could be clearly recognized up to the highest pressure studied here (Fig. 1b). Note that Adler and Williams (2005) used the mixture of 17% Fe_4N and 83% Fe_7N_3 as starting materials and the methanol-ethanol-water (MEW, 16 : 4 : 1) mixture as a pressure-transmitting medium. So, it can be speculated that the diffraction peaks of Fe_4N could have partly overlapped with Fe_7N_3. Another reason could be the non-hydrostatic nature of MEW at 30 GPa, as it is known to solidify by 15.2 GPa (Klotz et al., 2009).

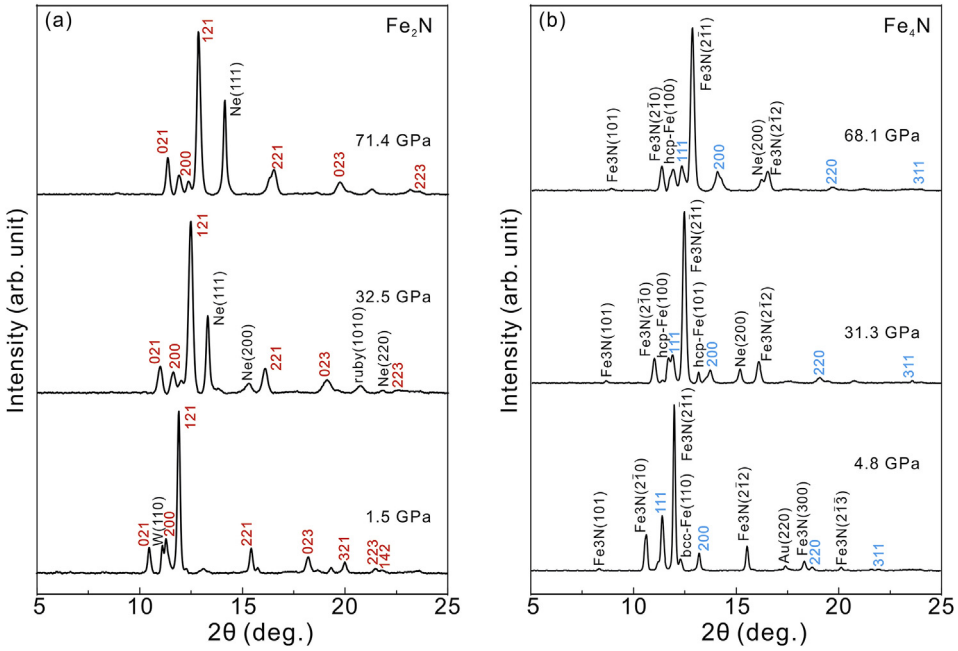

Fig. 1. Representative XRD patterns of iron nitrides Fe_2N and Fe_4N with pressure. Red labels in Fig. 1a are the peaks of Fe_2N while the blue ones in Fig. 1b are the peaks of Fe_4N. Both Au and ruby were used as pressure calibrants. The pressure medium was neon (Ne) and the gasket was tungsten (W) (λ = 0.4340 Å).

The volume of iron nitrides (Fe_2N and Fe_4N) are plotted as a function of pressure in Fig. 2a and b, respectively. Interestingly, the volume of Fe_2N showed a change at 10–20 GPa (Fig. 2a). However, the crystal structure of Fe_2N remained the same up to 71 GPa (Fig. 1a). This could be associated with an isostructural phase transition in Fe_2N at 10–20 GPa. In Fig. 3, the c/a and b/a values of Fe_2N were plotted against pressure. Fig. 3 gives more apparent evidence of discontinuity at about 10 GPa in both c/a and b/a ratios, which can be correlated with an isostructural transition. The Raman spectra (Figs. S2 and S3) also showed that Raman shifts of modes 1 and 2 displayed subtle changes at approximately 9 GPa, while the discontinuity in the Raman mode 3 is more obvious. These results indicated an isostructural phase transition in Fe_2N around 10–20 GPa, which is likely associated with a magnetic moment collapse or electron spin transition of iron in Fe_2N.

Lattice parameters of Fe_2N and Fe_4N are plotted as a function of pressure in Fig. 4. In orthorhombic Fe_2N, the lattice parameter a showed the largest reduction of 9.2% at ~50 GPa, whereas the b and c parameters reduced by 6.4% and 5.8%, respectively. It indicates the strong anisotropic effect of pressure on the a-axis of Fe_2N. The reduction of a-parameter in cubic Fe_4N was 6.2%, suggesting a lower reduction than the Fe_2N, indicating that Fe_4N may be more stable in the high-pressure area.

The EOS parameters of Fe_2N and Fe_4N were derived by fitting the P–V data to the third-order Birch-Murnaghan EOS, see Fig. 2. Fitting parameters for Fe_2N are as follows; the bulk modulus is $K_0 = 131.1(1)$ GPa with $V_0/Z = 29.6(1)$ Å^3 with a fixed K' at 4 at 0–10 GPa before the phase transition, and at 20–65 GPa the bulk modulus is $K_0 = 149.5(1)$ GPa with $V_0/Z = 28.8(1)$ Å^3 with a fixed K' at 4. Fitting parameters for Fe_4N are as follows; the bulk modulus is $K_0 = 144.4(1)$ GPa with $V_0/Z = 55.3(1)$ Å^3 with a fixed K' at 4.

In Fig. 5, the compressibility of Fe_2N and Fe_4N was plotted and compared with reported compressibility of other iron nitrides such as Fe_7N_3 and $Fe_3N_{1.26}$ (Adler and Williams, 2005; Litasov et al., 2017). In Fig. 5, it can be inferred that the compressibility of those iron nitrides is comparable. Furthermore, in Fig. 5, the compressibility of Fe_2N and Fe_4N is also compared with the compressibility of hcp-Fe and iron carbides such as Fe_7C_3, Fe_2C, and Fe_3C (Litasov et al., 2015). Iron nitrides are generally more compressible than hcp-Fe and the iron carbides, indicating the relatively strong effect of nitrogen on the enhancement of the compressibility of iron compared to carbon.

The pressure-dependent densities of the Fe_2N and Fe_4N samples were

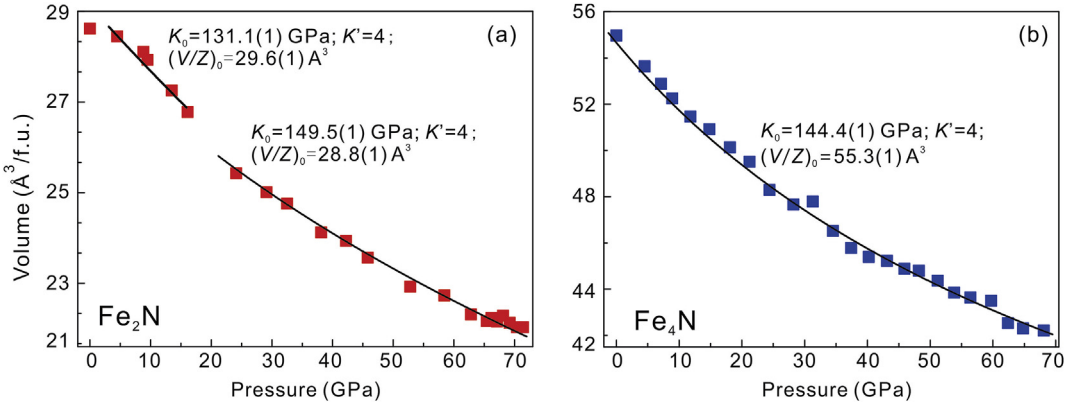

Fig. 2. The volume changes of Fe_2N and Fe_4N with pressure. The error bars are smaller than the symbols. The third-order Birch-Murnaghan fits to the data are shown by the solid curves.

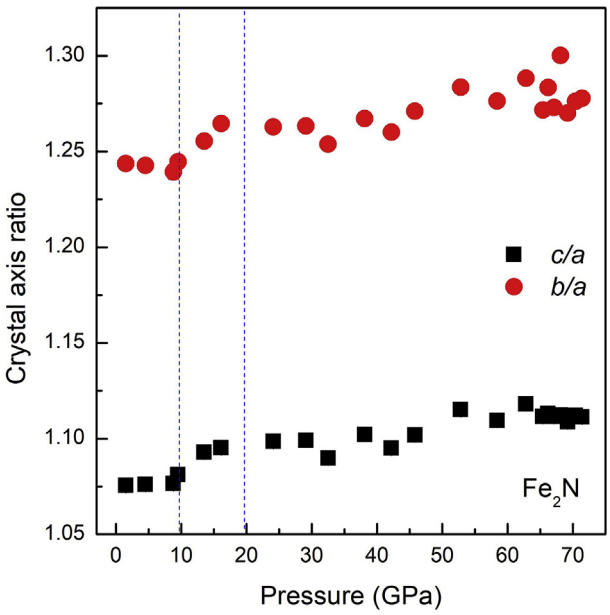

Fig. 3. The c/a and b/a changes of orthorhombic Fe_2N versus pressure. The error bars are smaller than the symbols. The dotted lines are the auxiliary lines.

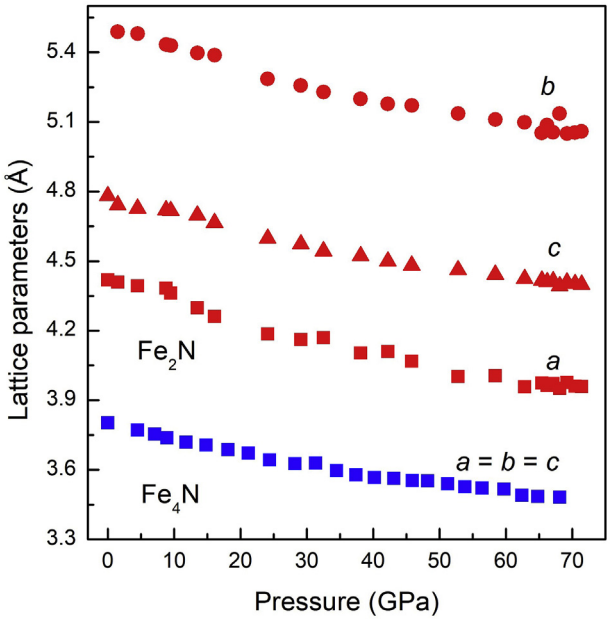

Fig. 4. The lattice parameters of Fe_2N and Fe_4N as a function of pressure. The error bars are smaller than the symbols.

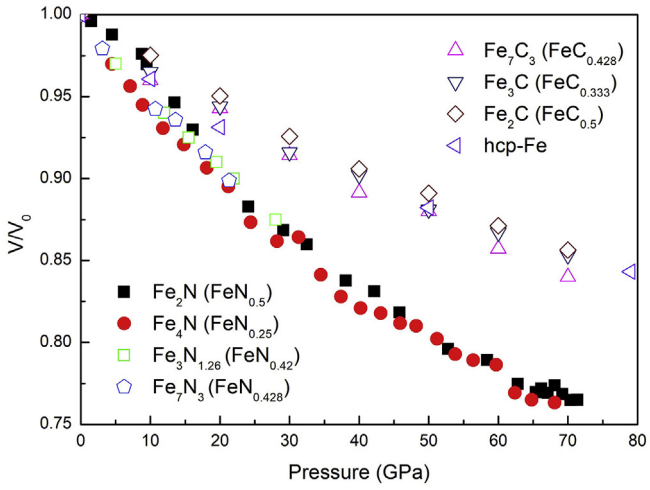

Fig. 5. The compression behaviour of Fe_2N and Fe_4N in comparison with other iron nitrides and carbide. The error bars are smaller than the symbols. Solid squares: Fe_2N (this study); solid circles: Fe_4N (this study); open squares: $Fe_3N_{1.26}$ (Litasov et al., 2017); open pentagon: Fe_7N_3 (Adler et al., 2005); open triangles, inverted triangles, diamonds and oblique triangles: Fe_7C_3, Fe_3C, Fe_2C and hcp-Fe, respectively (Litasov et al., 2015).

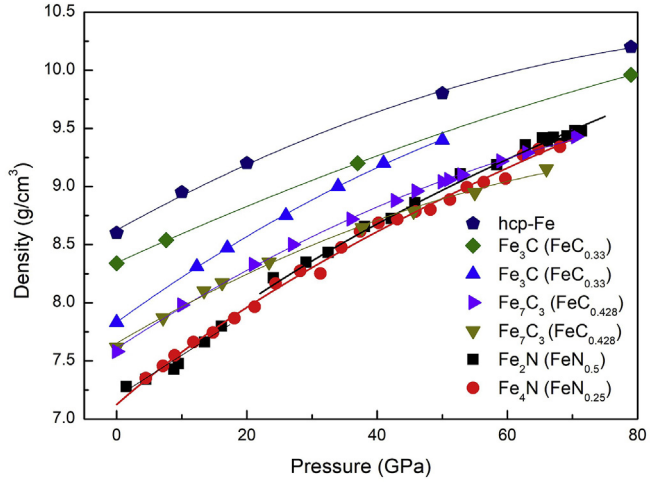

Fig. 6. The density of iron nitrides and carbides as a function of pressure. The solid curves represent fits to the data and extrapolations on the basis of the Birch-Murnaghan EOS. The error bars are smaller than the symbols. Squares: Fe_2N (this study); circles: Fe_4N (this study); diamonds: Fe_3C (Mookherjee et al., 2011); triangles: Fe_3C (Gao et al., 2008); oblique triangles: Fe_7C_3 (Prescher et al., 2015); inverted triangles: Fe_7C_3 (Chen et al., 2014); and pentagon: hcp-Fe (Mao et al., 1990).

plotted in Fig. 6. The densities of hcp-Fe, Fe_3C, Fe_7C_3, and Fe_2C are also plotted in Fig. 6. The densities of both iron nitrides are comparable. The effect of the nitrogen content on the density of iron-based nitrides seems to be constant at this stoichiometric range. The densities of iron nitrides were lower than those iron carbides (Fe_3C, Fe_7C_3, and Fe_2C) (Gao et al., 2008; Mookherjee, 2011; Nakajima et al., 2011; Chen et al., 2014; Litasov et al., 2015; Prescher et al., 2015). Thus, like compressibility, nitrogen can more significantly affect the density of iron compared to carbon (Mao et al., 1990). The nitrogen element itself plays an important role in affecting the properties of iron rather than its content per iron atom. We also speculate that compared to carbon, lower nitrogen content can explain the ~10% density deficit of the outer liquid core and the 3%–5% density deficit of the solid inner core in comparison to the experimentally-derived density of iron with seismological data.

3.2. *Electrical and thermal conductivity of Fe_2N at high pressure*

The electrical conductivity of Fe_2N was plotted against pressure in Fig. 7. The conductivities of iron nitrides were measured to be as low as 2–3 × 10^3 S m^{-1} at ambient pressure, which is consistent with some previous reports (Jiang and Jiang, 2019; Tao et al., 2019). Further, it is observed that the electrical conductivity of Fe_2N decreased at 0–10 GPa and increased after 10 GPa. This observation is consistent with volume discontinuity observed for Fe_2N in high-pressure XRD studies (Fig. 2a).

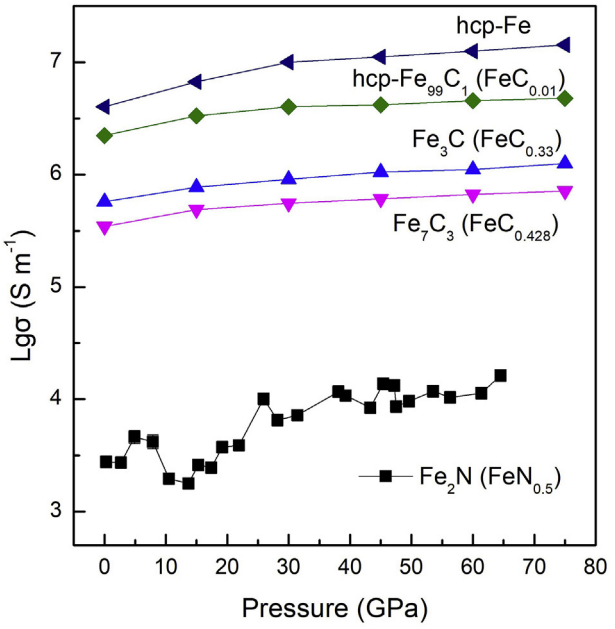

Fig. 7. The electrical conductivity of Fe_2N with pressure. The error bars are smaller than the symbols. Squares: Fe_2N (this study); inverted triangles, triangles, diamonds, and oblique triangles: Fe_7C_3, Fe_3C, hcp-$Fe_{99}C_1$, and hcp-Fe, respectively (Zhang et al., 2018).

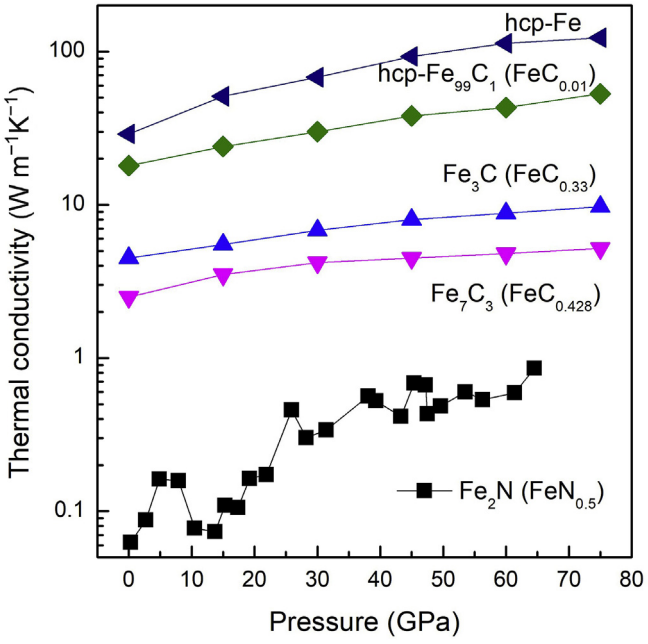

Fig. 8. The pressure-dependent thermal conductivity of Fe_2N. The data were converted from relative electrical conductivity using Wiedemann-Franz law at 300 K. The symbols are the same as Fig. 7. The error bars are smaller than the symbols.

In Fig. 7, we also compare the conductivity of Fe_2N with the reported electrical conductivity of hcp-Fe, Fe_7C_3, Fe_3C, and $Fe_{99}C_1$ (Zhang et al., 2018). These results indicate that the nitrogen can have a more significant effect on iron than carbon. Nitrogen shows a much stronger alloying effect on the electrical conductivity of iron than carbon. Further, the conductivity of Fe_2N increased gradually with pressure. With extrapolation to higher pressure, the conductivity of Fe_2N would be close to other iron-carbon alloys, which suggest the strong effect of pressure on the conductivity of iron nitrides compared to other iron alloys (Zhang et al., 2018). Pressure also has a significant effect on the solubility of nitrogen in iron (Mysen, 2019).

Electronic contribution plays a key role in the thermal and electrical conductivity of metals. Hence, the thermal conductivity of metals can be estimated from its electrical conductivity, using the Wiedemann-Franz law (Anzellini et al., 2013): $k_e = L\sigma T$. Where k_e is the thermal conductivity contributed by electrons, L is the Lorenz number, σ is the electrical conductivity, T is the temperature, and L is usually adopted by the ideal value ($L_0 = 2.44 \times 10^{-8}$ W Ω K^{-2}) at high pressure and temperature (Gomi and Hirose, 2015; Ohta et al., 2016). The thermal conductivity of Fe_2N is calculated using the same approach and is plotted in Fig. 8. Similar to electrical conductivity (Fig. 7), nitrogen can significantly decrease the thermal conductivity of iron, and like other physical properties, the nitrogen element also has a significant influence on the thermodynamic properties of iron compared to carbon.

3.3. Iron nitrides and carbides in the deep earth

As substantial studies have been carried out on nitrogen in the deep Earth, the decision to rule out the nitrogen element as a light element in the deep mantle and core seems an arbitrary choice. Our XRD results show that both the mainstream iron nitrides Fe_2N and Fe_4N can be thermodynamically stable at high pressure. Compared to carbon in iron phases under high pressure, nitrogen showed a stronger effect on the geophysical properties of iron. Nitrogen can effectively decrease the density and the electrical and thermal conductivity of iron with relatively lower content. Thus, nitrogen could coexist with other light elements in the deep Earth.

Otherwise, it is plausible that carbon plays an important role in the deep Earth with iron. We compared Fe_2N and Fe_4N with different iron carbides and found they are interestingly similar to each other, further proving that iron nitrides can be solid solutions in iron carbides at high pressure (Schnepp et al., 2015; Litasov et al., 2016). This fact may have potentially significant implications that the carbon content is lower than previous predictions in the deep Earth with nitrogen to achieve the goal of seismological features observed in the Earth's lower mantle and core. Iron-nitride exhibited higher stability at high pressure. Thus, iron-carbide can be replaced by iron-nitride through the reaction of N-bearing fluid with iron-carbide due to their very close structural similarity, and the N, itself, is siderophile under reducing conditions (Johnson and Goldblatt, 2015; Litasov et al., 2017). Actually, previous studies about inclusions in diamonds have revealed that up to 20 mol.% carbon can be replaced by nitrogen in iron-carbides (Kaminsky et al., 2015; Smith et al., 2016).

Many studies have proved that nitrogen content is greatly underestimated in the deep Earth (Johnson and Goldblatt, 2015; Yoshioka et al., 2018). Through the Earth's history, nitrogen stored in the mantle and core may have increased based on the deduction for the difference in nitrogen input and output (Mysen, 2019). Subduction zones can slide into the mantle, even the core (Mao et al., 2017), and have proven to be major venues for nitrogen flux into and out of the Earth (Busigny et al., 2011). Moreover, lots of previous studies indicate a variety of minerals can be effective carriers to bringing nitrogen into the deep Earth through subduction zones such as clay minerals (Cedeño et al., 2019), mica (Sokol et al., 2018) and feldspar (Watenphul et al., 2009). Our experimental results clearly show the significant effect of nitrogen on the compressibility, density, electrical, and thermal conductivity of iron. The effect of carbon content on iron was noticeable, while the effect of nitrogen was subtle. However, the nitrogen element has a more remarkable influence on the thermodynamic properties of iron compared to the carbon element at high pressure. Nitrogen could exist in the deep Earth as many forms of iron nitrides or solid solutions of iron carbides. Therefore, it is desirable to study the behaviors of nitrogen and its derivatives in the Earth's deep interior further.

4. Conclusions

In summary, synchrotron XRD and electrical conductivity studies were carried out for Fe_2N and Fe_4N in DACs up to ~70 GPa at ambient temperature. XRD and electrical conductivity experiments confirmed the isostructural phase transition in Fe_2N at 10–20 GPa. Fe_4N has no structural transition in the experimentally investigated pressure range. For Fe_2N EOS fitting parameters are as, $K_0 = 131.1(1)$ GPa, $V_0/Z = 29.6(1)$ Å^3, K' fixed at 4 for 0–10 GPa range and $K_0 = 149.5(1)$ GPa, $V_0/Z = 28.8(1)$ Å^3, K' fixed at 4 for 20–65 GPa range. For Fe_4N the EOS fitting parameters are as, $K_0 = 144.4(1)$ GPa, $V_0/Z = 55.3(1)$ Å^3, K' at 4.

The density, compressibility, and electrical and thermal conductivity of iron nitrides at high pressures were compared with iron carbides. Iron nitrides displayed lower density, higher compressibility, and much lower electrical and thermal conductivity than iron carbides. Thus, nitrogen would have a more remarkable influence on the high-pressure properties of iron than carbon. Our work also shows nitrogen itself plays an important role in affecting the properties of iron rather than its content per iron atom. The present results indicate that the role that nitrogen plays in the deep Earth has been previously underestimated and should be reevaluated.

Declaration of competing interest

The authors declare that they have no known competing financial interests or personal relationships that could have appeared to influence the work reported in this paper.

Acknowledgements

We acknowledge the use of synchrotron X-ray diffraction at the 13BM-C of GSECARS, Advanced Photon Sciences, Argonne National Laboratory. Yukai Zhuang is supported by the China Postdoctoral Science Foundation (18NZ021-0213-216308). GeoSoilEnviroCARS is supported by the National Science Foundation- Earth Sciences (EAR – 1634415) and the Department of Energy-GeoSciences (DE-FG02-94ER14466). 13BM-C is partially supported by COMPRES under NSF Cooperative Agreement EAR -1606856. This research used resources of the Advanced Photon Source, a U.S. Department of Energy (DOE) Office of Science User Facility operated for the DOE Office of Science by Argonne National Laboratory under Contract No. DE-AC02-06CH11357.

Appendix A. Supplementary data

Supplementary data to this article can be found online at https://doi.org/10.1016/j.gsf.2020.04.012.

References

Adler, J.F., Williams, Q., 2005. A high-pressure X-ray diffraction study of iron nitrides: implications for Earth's core. J. Geophys. Res. 110, B01203.
Allègre, C., Manhès, G., Lewin, É., 2001. Chemical composition of the Earth and the volatility control on planetary genetics. Earth Planet Sci. Lett. 185, 49–69.
Anzellini, S., Dewaele, A., Mezouar, M., Loubeyre, P., Morard, G., 2013. Melting of iron at Earth's inner core boundary based on fast X-ray diffraction. Science 340, 464–466.
Bebout, G.E., Fogel, M.L., Cartigny, P., 2013. Nitrogen: highly volatile yet surprisingly compatible. Elements 9, 333–338.
Bebout, G.E., Penniston-Dorland, S.C., 2016. Fluid and mass transfer at subduction interfaces—the field metamorphic record. Lithos 240–243, 228–258.
Busigny, V., Cartigny, P., Philippot, P., 2011. Nitrogen isotopes in ophiolitic metagabbros: a re-evaluation of modern nitrogen fluxes in subduction zones and implication for the early Earth atmosphere. Geochem. Cosmochim. Acta 75, 7502–7521.
Cartigny, P., 2005. Stable isotopes and the origin of diamond. Elements 1, 79–84.
Cedeño, D.G., Conceição, R.V., Souza, M.R.W., Quinteiro, R.V.S., Carniel, L.C., Ketzer, J.M.M., Rodrigues, F., Bruzza, E.C., 2019. An experimental study on smectites as nitrogen conveyors in subduction zones. Appl. Clay Sci. 168, 1–6.
Chen, B., Li, Z., Zhang, D., Liu, J., Hu, M.Y., Zhao, J., Bi, W., Alp, E.E., Xiao, Y., Chow, P., Li, J., 2014. Hidden carbon in Earth's inner core revealed by shear softening in dense Fe_7C_3. Proc. Natl. Acad. Sci. U.S.A. 111, 17755–17758.
Chen, Q., Zhang, Z., Wang, Z., Li, W.-C., Gao, X.-Y., Ni, H., 2019. In situ Raman spectroscopic study of nitrogen speciation in aqueous fluids under pressure. Chem. Geol. 506, 51–57.
Eugster, H.P., Munoz, J., 1966. Ammonium micas: possible sources of atmospheric ammonia and nitrogen. Science 151, 683–686.
Gao, L., Chen, B., Wang, J., Alp, E.E., Zhao, J., Lerche, M., Sturhahn, W., Scott, H.P., Huang, F., Ding, Y., Sinogeikin, S.V., Lundstrom, C.C., Bass, J.D., Li, J., 2008. Pressure-induced magnetic transition and sound velocities of Fe_3C: implications for carbon in the Earth's inner core. Geophys. Res. Lett. 35, L17306.
Gomi, H., Hirose, K., 2015. Electrical resistivity and thermal conductivity of hcp Fe–Ni alloys under high pressure: implications for thermal convection in the Earth's core. Phys. Earth Planet. In. 247, 2–10.
Halliday, A.N., 2013. The origins of volatiles in the terrestrial planets. Geochem. Cosmochim. Acta 105, 146–171.
Ishimatsu, N., Maruyama, H., Kawamura, N., Suzuki, M., Ohishi, Y., Ito, M., Nasu, S., Kawakami, T., Shimomura, O., 2003. Pressure-induced magnetic transition in Fe_4N probed by FeK-edge XMCD measurement. J. Phys. Soc. Jpn. 72, 2372–2376.
Jacobs, H., Rechenbach, D., Zachwieja, U., 1995. Structure determination of γ'-Fe_4N and ε-Fe_3N. J. Alloys Compd. 227, 10–17.
Javoy, M., 1997. The major volatile elements of the Earth: their origin, behavior, and fate. Geophys. Res. Lett. 24, 177–180.
Jiang, Y., Jiang, L., 2019. Synthesis of γ-Fe_4N soft magnetic material by high-pressure nitriding approach. IEEE Trans. Magn. 55, 1–4.
Johnson, B., Goldblatt, C., 2015. The nitrogen budget of Earth. Earth Sci. Rev. 148, 150–173.
Kaminsky, F.V., Wirth, R., Schreiber, A., 2015. A microinclusion of lower-mantle rock and other minerals and nitrogen lower-mantle inclusions in a diamond. Can. Mineral. 53, 83–104.
Kaminsky, F., Wirth, R., 2017. Nitrides and carbonitrides from the lowermost mantle and their importance in the search for Earth's "lost" nitrogen. Am. Mineral. 102, 1667–1676.
Klotz, S., Chervin, J.C., Munsch, P., Le Marchand, G., 2009. Hydrostatic limits of 11 pressure transmitting media. J. Phys. Appl. Phys. 42, 075413.
Kusakabe, M., Hirose, K., Sinmyo, R., Kuwayama, Y., Ohishi, Y., Helffrich, G., 2019. Melting curve and equation of state of β-Fe_7N_3: nitrogen in the Core? J. Geophys. Res.: Solid Earth 124, 3448–3457.
Laniel, D., Dewaele, A., Anzellini, S., Guignot, N., 2018. Study of the iron nitride FeN into the megabar regime. J. Alloys Compd. 733, 53–58.
Lécuyer, C., Simon, L., Guyot, F., 2000. Comparison of carbon, nitrogen and water budgets on Venus and the Earth. Earth Planet Sci. Lett. 181, 33–40.
Li, Y., Vočadlo, L., Brodholt, J., Wood, I.G., 2016. Thermoelasticity of Fe_7C_3 under inner core conditions. J. Geophys. Res.: Solid Earth 121, 5828–5837.
Litasov, K.D., Popov, Z.I., Gavryushkin, P.N., Ovchinnikov, S.G., Fedorov, A.S., 2015. First-principles calculations of the equations of state and relative stability of iron carbides at the Earth's core pressures. Russ. Geol. Geophys. 56, 164–171.
Litasov, K.D., Shatskiy, A.F., Ohtani, E., 2016. Interaction of Fe and Fe_3C with hydrogen and nitrogen at 6–20 GPa: a study by in situ X-ray diffraction. Geochem. Int. 54, 914–921.
Litasov, K.D., Shatskiy, A.F., Ovchinnikov, S.G., Popov, Z.I., Ponomarev, D.S., Ohtani, E., 2014. Phase transformations of Fe_3N-Fe_4N iron nitrides at pressures up to 30 GPa studied by in situ X-ray diffractometry. JETP Lett. (Engl. Transl.) 98, 805–808.
Litasov, K.D., Shatskiy, A., Ponomarev, D.S., Gavryushkin, P.N., 2017. Equations of state of iron nitrides ε-Fe_3N_x and γ-Fe_4N_y to 30 GPa and 1200 K and implication for nitrogen in the Earth's core. J. Geophys. Res.: Solid Earth 122, 3574–3584.
Mao, H.K., Hu, Q., Yang, L., Liu, J., Kim, D.Y., Meng, Y., Zhang, L., Prakapenka, V.B., Yang, W., Mao, W.L., 2017. When water meets iron at Earth's core–mantle boundary. National Sci. Rev. 4, 870–878.
Mao, H.K., Wu, Y., Chen, L.C., Shu, J.F., Jephcoat, A.P., 1990. Static compression of iron to 300 GPa and $Fe_{0.8}Ni_{0.2}$ alloy to 260 GPa: implications for composition of the core. J. Geophys. Res. 95, 21737–21742.
Mao, H.K., Xu, J., Bell, P.M., 1986. Calibration of the ruby pressure gauge to 800 kbar under quasi-hydrostatic conditions. J. Geophys. Res. 91, 4673–4676.
Mikhail, S., Sverjensky, D.A., 2014. Nitrogen speciation in upper mantle fluids and the origin of Earth's nitrogen-rich atmosphere. Nat. Geosci. 7, 816–819.
Minobe, S., Nakajima, Y., Hirose, K., Ohishi, Y., 2015. Stability and compressibility of a new iron-nitride β-Fe_7N_3 to core pressures. Geophys. Res. Lett. 42, 5206–5211.
Mookherjee, M., 2011. Elasticity and anisotropy of Fe_3C at high pressures. Am. Mineral. 96, 1530–1536.
Moore, C.B., Gibson Jr., E.K., Keil, K., 1969. Nitrogen abundances in enstatite chondrites. Earth Planet Sci. Lett. 6, 457–460.
Mysen, B., 2019. Nitrogen in the Earth: abundance and transport. Prog. Earth Planet. Sci. 6, 38.
Nakajima, Y., Takahashi, E., Sata, N., Nishihara, Y., Hirose, K., Funakoshi, K.I., Ohishi, Y., 2011. Thermoelastic property and high-pressure stability of Fe_7C_3: implication for iron-carbide in the Earth's core. Am. Mineral. 96, 1158–1165.
Nielsen, H.P., Buchwald, V.F., 1981. Roaldite, a new nitride in iron meteorites. Lunar Planet Sci. Conf. Proc. 12B, 1343–1348.
Ohta, K., Kuwayama, Y., Hirose, K., Shimizu, K., Ohishi, Y., 2016. Experimental determination of the electrical resistivity of iron at Earth's core conditions. Nature 534, 95–98.
Owen, T., Biemann, K., Rushneck, D.R., Biller, J.E., Howarth, D.W., Lafleur, A.L., 1977. The composition of the atmosphere at the surface of Mars. J. Geophys. Res. 82, 4635–4639.
Prescher, C., Dubrovinsky, L., Bykova, E., Kupenko, I., Glazyrin, K., Kantor, A., McCammon, C., Mookherjee, M., Nakajima, Y., Miyajima, N., Sinmyo, R., Cerantola, V., Dubrovinskaia, N., Prakapenka, V., Rüffer, R., Chumakov, A.,

Hanfland, M., 2015. High Poisson's ratio of Earth's inner core explained by carbon alloying. Nat. Geosci. 8, 220–223.
Prescher, C., Prakapenka, V.B., 2015. DIOPTAS: a program for reduction of two-dimensional X-ray diffraction data and data exploration. High Pres. Res. 35, 223–230.
Rubin, A.E., 1997. Mineralogy of meteorite groups. Meteoritics Planet Sci. 32, 231–247.
Sagatov, N., Gavryushkin, P.N., Inerbaev, T.M., Litasov, K.D., 2019. New high-pressure phases of Fe_7N_3 and Fe_7C_3 stable at Earth's core conditions: evidences for carbon–nitrogen isomorphism in Fe-compounds. RSC Adv. 9, 3577–3581.
Schnepp, Z., Danks, A.E., Hollamby, M.J., Pauw, B.R., Murray, C.A., Tang, C.C., 2015. In Situ synchrotron X-ray diffraction study of the Sol–Gel synthesis of Fe_3N and Fe_3C. Chem. Mater. 27, 5094–5099.
Smith, E.M., Shirey, S.B., Nestola, F., Bullock, E.S., Wang, J., Richardson, S.H., Wang, W., 2016. Large gem diamonds from metallic liquid in Earth's deep mantle. Science 354, 1403–1405.
Sokol, A.G., Kruk, A.N., Seryotkin, Y.V., Korablin, A.A., Palyanov, Y.N., 2017a. Phase relations in the Fe-Fe_3C-Fe_3N system at 7.8 GPa and 1350 °C: implications for carbon and nitrogen hosts in Fe^0-saturated upper mantle. Phys. Earth Planet. In. 265, 43–53.
Sokol, A.G., Palyanov, Y.N., Tomilenko, A.A., Bul'bak, T.A., Palyanova, G.A., 2017b. Carbon and nitrogen speciation in nitrogen-rich C–O–H–N fluids at 5.5–7.8 GPa. Earth Planet Sci. Lett. 460, 234–243.
Sokol, A.G., Sokol, E.V., Kupriyanov, I.N., Sobolev, N.V., 2018. Synthesis of NH_4-substituted muscovite at 6.3 GPa and 1000°C: implications for nitrogen transport to the Earth's mantle. Dokl. Earth Sci. 479, 404–407.
Sugiura, N., 1998. Ion probe measurements of carbon and nitrogen in iron meteorites. Meteoritics Planet Sci. 33, 393–409.
Sugiura, N., Kiyota, K., Hashizume, K., 1998. Nitrogen components in primitive ordinary chondrites. Meteoritics Planet Sci. 33, 463–482.
Tao, Z., Liu, S., Fang, H., Chen, L., Chen, J., Xiu, X., Zhang, R., 2019. Magnetic and transport properties of single-phase N-rich iron nitrides. Mater. Lett. 239, 140–142.
Tessier, F., Navrotsky, A., Niewa, R., Leineweber, A., Jacobs, H., Kikkawa, S., Takahashi, M., Kanamaru, F., DiSalvo, F.J., 2000. Energetics of binary iron nitrides. Solid State Sci. 2, 457–462.
van der Pauw, L.J., 1958. A method of measuring specific resistivity and Hall effect of discs of arbitrary shape. Philips Res. Rep. 13, 1–9.
Watenphul, A., Wunder, B., Heinrich, W., 2009. High-pressure ammonium-bearing silicates: implications for nitrogen and hydrogen storage in the Earth's mantle. Am. Mineral. 94, 283–292.
Watenphul, A., Wunder, B., Wirth, R., Heinrich, W., 2010. Ammonium-bearing clinopyroxene: a potential nitrogen reservoir in the Earth's mantle. Chem. Geol. 270, 240–248.
Ye, Y., Shim, S.-H., Prakapenka, V., Meng, Y., 2018. Equation of state of solid Ne inter-calibrated with the MgO, Au, Pt, NaCl-B_2, and ruby pressure scales up to 130GPa. High Pres. Res. 38, 377–395.
Yoshioka, T., Wiedenbeck, M., Shcheka, S., Keppler, H., 2018. Nitrogen solubility in the deep mantle and the origin of Earth's primordial nitrogen budget. Earth Planet Sci. Lett. 488, 134–143.
Zhang, C., Lin, J.-F., Liu, Y., Feng, S., Jin, C., Hou, M., Yoshino, T., 2018. Electrical resistivity of Fe-C alloy at high pressure: effects of carbon as a light element on the thermal conductivity of the Earth's core. J. Geophys. Res.: Solid Earth 123, 3564–3577.